Network Anatomy and *In Vivo* Physiology of Visual Cortical Neurons

Davi D. Bock, PhD[1,2]; Wei-Chung Allen Lee, PhD[1,2]; Aaron M. Kerlin, PhD[1]; Mark L. Andermann, PhD[1]; Greg Hood, MS[3]; Arthur W. Wetzel, PhD[3]; Sergey Yurgenson, PhD[1]; Edward R. Soucy, PhD[2]; Hyon Suk Kim[1,2]; and R. Clay Reid, MD, PhD[1,2]

[1]Department of Neurobiology
Harvard Medical School
Boston, Massachusetts

[2]The Center for Brain Science
Harvard University
Cambridge, Massachusetts

[3]National Resource for Biomedical Supercomputing
Pittsburgh Supercomputing Center
Carnegie Mellon University
Pittsburgh, Pennsylvania

NOTES

Introduction

In the cerebral cortex, local circuits consist of tens of thousands of neurons, each of which makes thousands of synaptic connections. Perhaps the biggest impediment to understanding these networks is that we have no wiring diagrams of their interconnections. Even if we had a partial or complete wiring diagram, however, understanding the network would also require information about each neuron's function.

In this chapter, we show that the relationship between structure and function can be studied in the cortex using a combination of *in vivo* physiology and network anatomy. We used two-photon calcium imaging to characterize a functional property — the preferred stimulus orientation — of a group of neurons in the mouse primary visual cortex. Large-scale electron microscopy (EM) of serial thin sections was then used to trace a portion of these neurons' local network. Consistent with a prediction from recent physiological experiments, inhibitory interneurons received convergent anatomical input from nearby excitatory neurons with a broad range of preferred orientations, although weak biases could not be rejected.

Past studies of the synaptic connections in the cortex have focused on a few cells at a time, so that today we have only partial information about the structure of highly interconnected cortical networks. Until recently, anatomists relied on the sparse labeling of individual neurons to trace the extensive axonal and dendritic arbors of cortical neurons. Synaptic connectivity was originally inferred from the overlap of axonal and dendritic arbors (Ramon y Cajal, 1904), an approach that remains fruitful today (Binzegger et al., 2004; Stepanyants, 2008). Combined physiological and anatomical studies of cortical slices *in vitro* have extended this analysis to include rules of pairwise connectivity between different cell types and cortical layers (Mason et al., 1991; Markram et al., 1997; Thomson and Bannister, 2003). It has been argued that the cortical network might be random beyond these simple statistical rules (Braitenberg and Schüz, 1998), but recent studies suggest that there could be higher-order patterns of connections in cortical networks, such as mutually interconnected triplets of cells (Song et al., 2005) and subnetworks of neurons that are highly connected within a group but not between groups (Yoshimura and Callaway, 2005; Yoshimura et al., 2005). Although these hypothesized patterns are based on *in vitro* physiological data, they have never been demonstrated anatomically, nor have they been related to information processing as measured from neural response properties *in vivo*.

EM is an ideal tool for characterizing the highly interconnected structure of cortical networks. From visualizing quantal release by synaptic vesicles (Heuser et al., 1979) to generating a complete wiring diagram of a model organism (White et al., 1986), it has provided definitive data for examining the relationship between structure and function in the nervous system. Electrophysiology, combined with light microscopy and serial-section EM, has allowed the inspection of structure-function relationships of single cells within neural circuits, such as the hippocampus (Sorra and Harris, 1998), retina (Sterling, 1983; Dacheux and Raviola, 1986), thalamus (Hamos et al., 1987), and cortex (Kisvárday et al., 1986; Anderson et al., 1994; Ahmed et al., 1997; Tamas et al., 1998). A crucial difference from light microscopy is that serial-section EM can be used

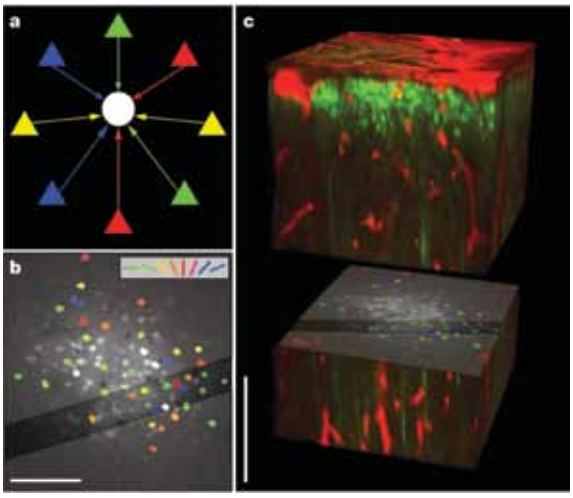

Figure 1. Functional characterization of neurons before anatomical reconstruction. ***a***, Schematic representation of diverse input to inhibitory interneurons. Excitatory pyramidal cells (triangles) with varied preferred orientations (different colors) provide input (colored arrows) to an inhibitory interneuron (white circle). ***b***, Cell-based visual orientation preference map in the mouse visual cortex from *in vivo* two-photon calcium imaging. Visually responsive cells are colored according to their estimated preferred orientation (color coding shown at top), with broadly tuned cells (orientation selectivity index ≤0.2) shown white. Dark diagonal band, region targeted for acquisition of EM sections, cut orthogonal to image plane. ***c***, *In vivo* two-photon fluorescence image of the three-dimensional volume (red, blood vessels or astrocytes; green, OGB-loaded somata or yellow fluorescent protein [YFP]–labeled apical dendrites) separated to expose the functionally imaged plane. Scale bars, 100 μm.

NOTES

to follow the three-dimensional contours of neuronal membranes, so that any given axon or dendrite can be traced over hundreds of micrometers without selective, sparse staining of individual neurons. This feature of serial-section EM has been used to examine small volumes of cortical tissue, typically numbering in the thousands of cubic micrometers, in which portions of multiple dendrites and axons were reconstructed to examine synaptic relationships among them (Shepherd and Harris, 1998; Anderson et al., 2009; Mishchenko et al., 2010).

Here we exploited recent improvements in computer speed and storage capacity to perform serial-section EM of a volume that encompasses millions of cubic micrometers, sufficient to contain large portions of the dendritic and axonal arbors of more than 1000 cells. With this dataset, we could attempt a sampling — targeted to a subset of functionally imaged cells — of the dense interconnections found in a cortical network. In particular, we tested a somewhat controversial prediction from recent physiological work (Sohya et al., 2007; Niell and Stryker, 2008; Liu et al., 2009; Kerlin et al., 2010; Ma et al., 2010; Runyan et al., 2010): that inhibitory interneurons in the mouse primary visual cortex receive dense, convergent input from nearby excitatory (pyramidal) neurons with widely varying preferred stimulus orientations (Fig. 1*a*).

Functional Imaging and Large-Scale EM

We used *in vivo* two-photon calcium imaging to determine the preferences for stimulus orientation of a cohort of cells in layer 2/3 of mouse primary visual

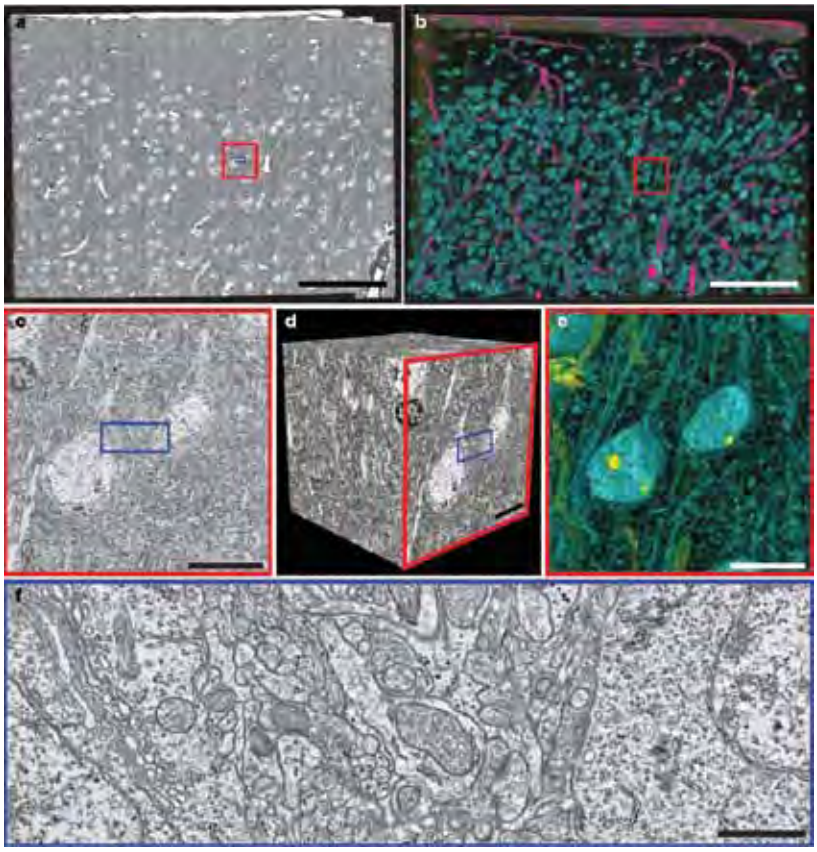

Figure 2. Large-scale EM. ***a***, Electron micrograph of an entire 120,000 × 80,000 pixel thin section, showing the pial surface (top) and cortical layers 1 through to upper 4 (bottom). ***b***, ***e***, Three-dimensional renderings of the EM volume through the entire series (***b***, supplementary Movie 3) and through 50 sections of the cube in ***d*** (***e***, red outline in ***b***, supplementary Movie 4). ***d***, A cube of the EM volume with ***c*** as one face. ***c***, ***f***, Zoomed-in view of 2 functionally characterized cells (***c***; red outline in ***a***) and the neuropile between them (***f***; blue outlines in ***a***, ***c*** and ***d***), illustrating the density of axons and dendrites coursing between cell bodies. Pink represents electron transparent regions (e.g., blood vessels), yellow represents regions that are electron dense (such as nucleoli, oligodendrocyte nuclei, and myelin), and aqua denotes regions with pixel values in between (e.g., nuclei, cell bodies, and dendrites). Scale bars: ***a***, ***b***, 100 μm; ***c***–***e***, 10 μm; ***f***, 1 μm.

NOTES

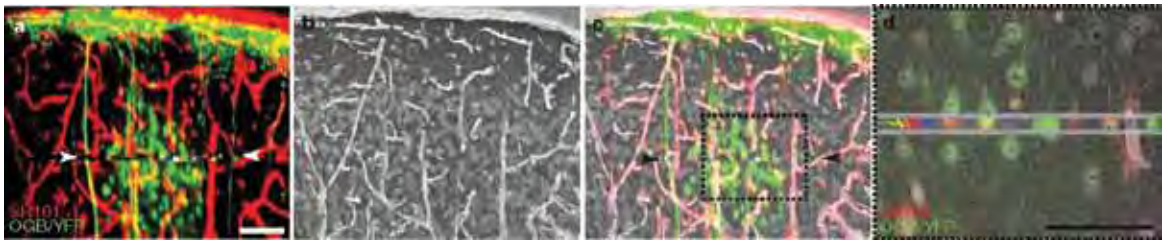

Figure 3. Correspondence between *in vivo* fluorescence anatomy and EM. ***a***, Maximum-intensity projection of the *in vivo* fluorescence anatomy corresponding to the EM volume (red, blood vessels or astrocytes; green, OGB or YFP, as in **Fig. 1*c***). Colors between arrowheads correspond to orientation preference of neurons in the imaged plane, as in ***d***. ***b***, Projection through 37 EM sections evenly spaced in the series. ***c***, Merge of EM and fluorescence projections. ***d***, Zoomed-in view of the region outlined in ***c***, showing the overlay of *in vivo* and EM data in a single thin section. Horizontal gray lines delineate the functionally imaged plane. Within the functionally imaged plane, the cell bodies of 6 neurons of known orientation preference (from left to right: cells 13, 12, 11, 10, 9, and 8, colored as in **Fig. 1*b***) are well registered with their EM ultrastructure. Outside the functionally imaged plane, blood vessels and astrocytes in the EM are well registered with the red SR101 staining. Scale bars, 50 μm.

cortex (Ohki et al., 2005; Kerlin et al., 2010). After loading cells with the fluorescent calcium indicator Oregon Green BAPTA-1 AM (OGB) (Stosiek et al., 2003), we recorded neuronal activity, as reflected by increases in intracellular calcium from a single plane of cells 186 mm beneath the brain surface. Black and white bars of varying orientations and directions were presented to the anaesthetized animal, and the cellular responses were used to generate a map of orientation preference (Fig. 1*b* and supplemental Fig. 1; Methods). We concluded the *in vivo* experiment by collecting a stack of images from a volume surrounding the calcium-imaged plane (Fig. 1*c*; red, vessels; green, neurons). We then immediately perfused the animal and prepared the corresponding volume of visual cortex for serial-section transmission EM (TEM; Methods).

After finding the calcium-imaged region of cortex (Methods), we cut a series of 1215 thin sections (40–45 nm), oriented radially, at right angles to the functionally imaged plane (Fig. 1*b*,*c*). Each section was wide enough (450 μm) to encompass the imaged plane, and tall enough (350 μm) to include cortical layers 1, 2/3, and upper 4 (Fig. 2*a*,*b*, supplemental Movie 1). Although cortical axons can travel for millimeters, the proximal axonal collaterals of pyramidal cells arborize more locally (Braitenberg and Schüz, 1998), such that a portion of their local connectivity could be sampled within the span of the EM volume. In line with previous work, we found that in order to reliably trace the finest neural processes and to identify chemical synapses (Fig. 2*f*, supplemental Movie 2), we needed <50 nm section thickness and <5 nm lateral resolution (Harris et al., 2006).

We built a custom TEM Camera Array (TEMCA) that used 4 high-speed charge-coupled device (CCD) cameras to efficiently acquire EM images of the required size and resolution (supplementary Fig. 2; Methods). The TEMCA achieves an order of magnitude increase in throughput over most commercially available TEM imaging systems. This system enabled us to collect the thousands of individual images required to mosaic each of the serial sections in approximately 20 min (Fig. 2*a*) so that we could image the entire series over the course of several months.

The 3.2×10^6 camera images in our dataset were converted into a seamless three-dimensional image volume by globally registering and aligning the EM volume after automated stitching of adjacent images into sections (Methods). The raw image data were approximately 36×10^{12} bytes (36 terabytes [TB]), with the final stitched and registered EM data set encompassing approximately 10 million megapixels (10 TB), spanning ~450 × 350 × 52 μm and containing approximately 1500 cell bodies (Fig. 2*b*).

We next relocated in the EM volume the cells whose function had been characterized by *in vivo* calcium imaging. The large extent of the EM dataset permitted registration of the fluorescently labeled vasculature and neurons between two-photon and EM imaging (Fig. 3*a*–*c*). We matched blood vessels of successively finer caliber, followed by the cell bodies, in order to identify individual neurons of known orientation selectivity within the EM volume (Fig. 3*d*, supplementary Fig. 3; Methods). The EM volume intersected the cell bodies of 14 visually responsive neurons (Fig. 1, supplementary Fig. 1). Thirteen of the cells were selective for stimulus orientation. The fourteenth neuron was visually responsive but nonselective for orientation. It had a nonpyramidal neuronal morphology, received asymmetric contacts

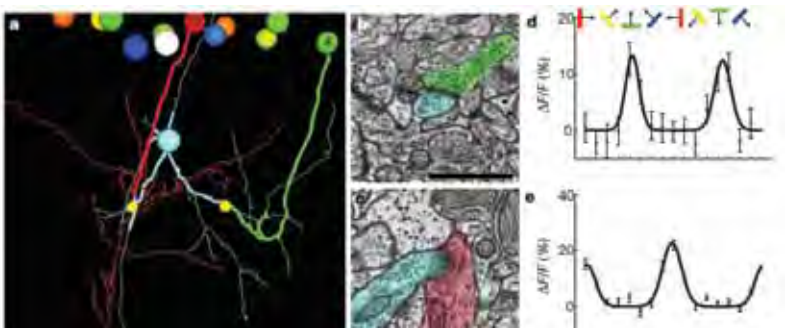

Figure 4. Convergent synaptic input onto inhibitory interneurons. ***a***, Three-dimensional rendering of axonal contacts onto a postsynaptic neuron. Large balls at the top represent cell bodies of neurons within the functionally imaged plane. Axons of a horizontally tuned neuron (cell 4; green) and a vertically tuned neuron (cell 10; red) descend and make synapses (small yellow balls) onto dendrites of an inhibitory interneuron (cyan). The axonal and dendritic segments leading to the convergence were independently traced by a second person, blind to the original segmentation (thick tracing). Cell bodies and axons colored by orientation preference, as in **Fig. 1*b***. Scale bar, 50 μm. ***b***, ***c***, Electron micrographs showing the synapses onto the inhibitory neuron from cell 4 (***b***) and cell 10 (***c***) with corresponding colors overlaid. Scale bar, 1 μm. ***d***, ***e***, Orientation tuning curves derived from *in vivo* calcium imaging of the cell bodies of cell 4 (***d***) and cell 10 (***e***). Colored bars and arrows, stimulus orientation and direction. Δ*F*/*F*, change in fluorescence. Error bars, +/– SEM.

onto the cell body, and made symmetric synapses onto its postsynaptic targets (supplementary Fig. 4), suggesting it was an inhibitory, GABAergic interneuron (Peters et al., 1991). Both the precision of physical registration and the alignment of appropriate functional properties with neuronal morphology (orientation-selective excitatory cells and an unselective inhibitory neuron) demonstrate that we successfully combined micrometer-scale *in vivo* functional imaging with nanometer-scale EM ultrastructure.

EM circuit reconstruction and the resultant network graph

To analyze the circuit's anatomical connectivity, we manually traced a wire-frame model of the dendritic and axonal arbors of each functionally characterized neuron and noted the location of each synapse along the axons. For each synapse, we then reconstructed the postsynaptic dendrite centripetally until we reached either the cell body or the boundary of the EM volume (Methods). In this directed manner, we were able to identify all of the postsynaptic targets that could be found in the EM-imaged volume and to determine when multiple axons converged onto a common postsynaptic target, without unnecessary tracing of the target cells' dendrites (Fig. 4, supplementary Fig. 5).

We categorized the postsynaptic targets as either excitatory or inhibitory on the basis of morphology. Pyramidal cell dendrites were densely studded with spines, whereas inhibitory interneuron dendrites were sparsely spinous and received more asymmetric (excitatory) synapses through their dendritic shafts (Peters et al., 1991). Of 245 synapses originating from 10 functionally characterized pyramidal neurons that made synapses in the EM-imaged volume, 125 (51%) were onto inhibitory dendrites and 120 (49%) onto excitatory dendrites. Of the 185 distinct postsynaptic targets, 71 (38%) were inhibitory (Fig. 5, cyan), and 114 (62%) were excitatory (Fig. 5, magenta). The proportion of inhibitory cells in the target population was less than the proportion of synapses onto inhibitory targets, because individual axons often made multiple synapses with inhibitory targets. We rendered the anatomical reconstructions of the functionally characterized cells and their postsynaptic targets as a graph (Fig. 5*b*) to examine the functional logic of the network.

Convergent excitatory input to inhibitory interneurons

In the graph of connectivity (Fig. 5*b*), we found multiple examples of pyramidal cells with diverse preferred stimulus orientations that provided convergent input to inhibitory neurons. We restricted subsequent analysis to a reduced and verified subnetwork that included convergent connections, as well as connections among the functionally imaged neurons (Fig. 5*c*,*d*, supplementary Figs. 6, 7; Methods). Most strikingly, some inhibitory targets received input from three or four distinct cells with a range of preferred orientations (Fig. 5*d*, supplementary Fig. 7*a–d*).

When we examined all of the convergences onto inhibitory targets, most were from pairs of cells that were close to each other (Figs. 5*c*, 6*a*), independent of the difference between their preferred orientations, which ranged from nearly orthogonal (Fig. 5*d*, center; supplementary Fig. 7*e–g*) to nearly identical (Fig. 5*d*, lower right; supplementary Fig. 7*m–o*). The strongest predictor of whether two axons converged on a common target was found by examining how many of their synapses were nearby in space (Fig. 6*b*,*c*; cumulative synaptic proximity, $p < 1.3 \times 10^{-5}$; Methods).

NOTES

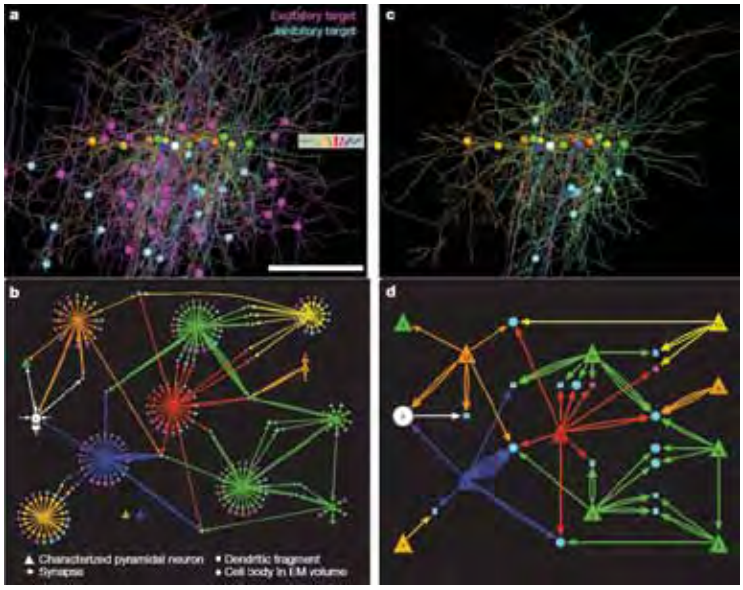

Figure 5. From anatomy to connectivity graphs. ***a***, Three-dimensional rendering of the dendrites, axons, and cell bodies of 14 neurons in the functionally imaged plane (colored according to their orientation preference, key right, as in **Fig. 1*b***), and the dendrites and cell bodies of all their postsynaptic targets traced in the EM volume (magenta, excitatory targets; cyan, inhibitory targets; spines on postsynaptic targets not shown; supplementary Movie 5). Scale bar, 100 μm. ***b***, Directed network diagram of the functionally characterized cells and their targets, derived from ***a***. Postsynaptic excitatory (magenta) and inhibitory (cyan) targets with cell bodies contained within the EM volume are drawn as circles. Other postsynaptic targets (dendritic fragments) are drawn as squares. (From top to bottom and left to right: functionally characterized cells 5, 2, 7; 13, 6, 14; 1; 10; 11, 3; 9; 12, 4; and 8.) ***c***, Three-dimensional rendering of the arbors and cell bodies of functionally characterized neurons, along with postsynaptic targets that either receive convergent input from multiple functionally characterized neurons, or were themselves functionally characterized (supplementary Movie 5). ***d***, A subset of the network graph showing only the connections in ***c***, all independently verified (from top to bottom and left to right: functionally characterized cells 5, 2, 7; 13, 6; 10; 11, 3; 12, 9, 8, and 4).

The functional properties of a pair of excitatory cells, specifically, the difference in their preferred orientations, were not predictive of whether they converged onto an inhibitory target. Pairs that converged had a distribution indistinguishable from the uniform distribution (Fig. 6*d*, red line; $p > 0.30$) and from a distribution in which all possible presynaptic pairs were considered, weighted by their proximity (Fig. 6*d*, blue line; $p > 0.68$; Methods). In summary, the axonal geometry of two excitatory neurons was a good predictor of whether they converged upon a nearby inhibitory interneuron, whereas the visual physiology of the excitatory neurons was not.

Discussion

The ability to study populations of neurons with a combination of network anatomy and *in vivo* physiology creates new opportunities for examining how neuronal circuits process information. Here we explored how both the geometry and the function of cortical neurons influence the patterns of connections between them. In the case of excitatory input to local inhibitory interneurons, geometry appeared to dominate over function (Braitenberg and Schüz, 1998). This finding may provide an anatomical substrate for a prediction from recent physiological studies of mouse visual cortex, in which inhibitory neurons were found to be less selective than excitatory neurons (Sohya et al., 2007; Niell and Stryker, 2008; Liu et al., 2009; Kerlin et al., 2010) (Fig. 1*a*), a finding that has been disputed for certain cell types by some groups (Ma et al., 2010; Runyan et al., 2010). Inhibitory interneurons that pool excitatory input could be used to set the gain of orientation–selective pyramidal cells (Liu et al., 2009, 2010; Alitto and Dan, 2010); they might also be involved in modulation of brain state (Alitto and Dan, 2010) or in attention-dependent normalization of cortical activity (Reynolds and Heeger, 2009).

Several studies have found that some subtypes of inhibitory neurons demonstrate orientation selectivity in the mouse (Ma et al., 2010; Runyan et al., 2010). We did not classify different subtypes of inhibitory neurons, and thus cannot rule out the possibility that some might receive more selective input. Furthermore, although our sample size was

NOTES

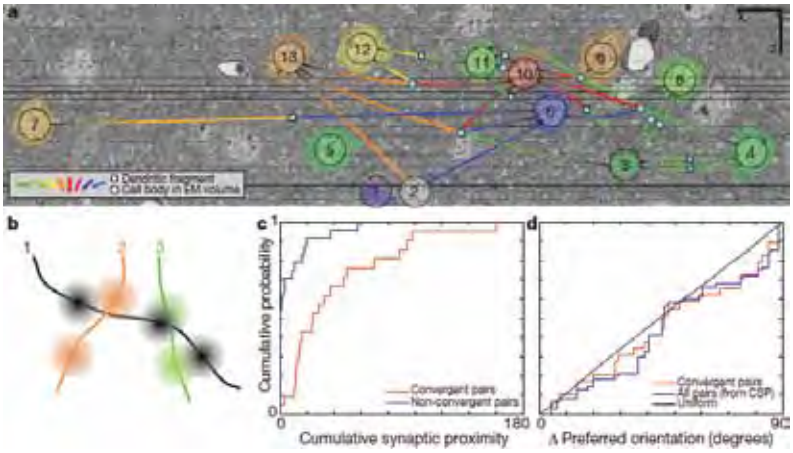

Figure 6. Convergent synaptic input onto inhibitory interneurons is predicted by proximity, not function. ***a***, A portion of the aligned and registered EM image series resliced parallel to the functionally imaged plane, through 1153 EM sections. Overlaid is a network graph of the convergences onto inhibitory interneurons. Visually responsive cell bodies are pseudo-colored according to their preferred orientation (as in **Fig. 1*b***) and numbered as in **Figs. 4** and **5**. Convergences onto inhibitory neuronal targets are represented by lines, corresponding to ≥1 synapses, leading either to filled cyan circles (targets traced to cell bodies in the EM volume) or squares (dendritic fragments). Cell 14 was partially contained in the EM volume and is not shown. Scale bars, 10 μm. ***b***, Diagram of CSP. Line segments represent axons, with three-dimensional Gaussians centered at each synapse. A CSP was calculated for each pair of orientation-tuned neurons by summing all pairwise overlaps of Gaussians from the 2 axons (σ = 12 μm; Methods). ***c***, Pairs of axons whose synaptic boutons were in close proximity were more likely to converge onto a common target. The CSP of axon pairs participating in convergences (red) was significantly greater than for nonconverging pairs (blue; $p < 1.3 \times 10^{-5}$; 2-sample Kolmogorov–Smirnov test; $n_{\text{convergent pairs}} = 21$; $n_{\text{nonconvergent pairs}} = 24$). ***d***, Convergences were not predicted by the difference in orientation preference between presynaptic cell pairs. The distribution of differences in orientation preference was not significantly different from a uniform distribution ($p > 0.30$; 2-sample Kolmogorov–Smirnov test; $n_{\text{convergences}} = 29$) or a model distribution (Methods) based on CSP ($p > 0.68$; 2-sample Kolmogorov-Smirnov test; $n_{\text{convergences}} = 29$).

large enough to exclude a strong bias in the preferred orientation tuning of convergent cell pairs, a larger sampling is necessary to exclude weaker biases (Methods).

Until it is possible to fully reconstruct large EM volumes (Helmstaedter et al., 2008; Mishchenko et al., 2010; Turaga et al., 2010), analysis of network connectivity will be limited to a partial sampling of the underlying anatomy. Here we concentrated on reconstructing the axons of functionally characterized pyramidal cells and their postsynaptic targets. Within our sample, we found that 51% of synapses were onto inhibitory targets, despite the preponderance of excitatory neurons in the cortex (Peters and Kara, 1985; White and Keller, 1989; Markram et al., 2004) and despite reports that 10–20% of the synapses made by pyramidal cells are onto inhibitory targets in cat (Kisvárday et al., 1986) and macaque (McGuire et al., 1991). Whether the higher percentage we observed is the result of a species difference (Thomson et al., 2002; Holmgren et al., 2003) or of the fact that we sampled synapses from proximal portions of the pyramidal cell axonal arbors, it resulted in our ability to sample a large number of convergences onto inhibitory targets (Fig. 5*d*).

Although the volume we imaged using EM was comparatively large, it proved to be near the minimum required to perform an analysis relating cortical function to network anatomy. We collected the series of wide-field (350 × 450 μm), high-resolution EM images to encompass the axonal arbors of the functionally characterized neurons and the dendrites of their targets. Nonetheless, we were limited by the shortest dimension in our volume (52 μm), determined by the number of thin sections, so we could trace only 245 out of the thousands of synapses made by the functionally characterized neurons.

We anticipate that the size of serial EM volumes will increase substantially in the near future, owing to increases in imaging throughput and series length made possible by automated techniques (Denk and Horstmann, 2004; Hayworth et al., 2006). The time required to trace connectivity between neurons is likely to remain a limiting factor, although semiautomated techniques have already achieved 10-fold increases in throughput over purely manual approaches (Mishchenko et al., 2010). For large-scale reconstruction, data quality is paramount. To trace unlabeled, fine-caliber axons, it is essential to have minimum section thickness, minimum section loss, and optimal tissue quality.

In the current study, we found a large number of convergent inputs onto inhibitory neurons principally because they were densely innervated by the excitatory axons we reconstructed. However, probing the network anatomy of more sparsely interconnected (and possibly weakly biased) (Jia

NOTES

et al., 2010) excitatory neurons (Ohki and Reid, 2007) will require larger samples. Here we sought to limit tissue damage from the infrared laser, so two-photon calcium imaging was confined to a single plane, or less than 1% of the cells in the volume (supplementary Fig. 8*a*). Recent advances in calcium imaging (Grewe and Helmchen, 2009; Tian et al., 2009), however, should now allow physiological data to be collected from many more cells in a volume while maintaining tissue quality.

It is fortunate that increases in the dimensions of an EM-imaged volume, and the number of physiologically characterized cells within it, produce combinatorial increases in the number of network motifs (Song et al., 2005) that can be analyzed in a single experiment (supplementary Fig. 8*b–d*). In particular, if a population of neurons is sparsely sampled, the number of interconnections found between them increases as the square of the sampling density. With moderate gains in the number of functionally imaged cells, or in the volumes encompassed by EM reconstructions, insight into the functional logic of cortical networks should therefore increase at an accelerating pace.

Methods Summary

We performed two-photon imaging in the mouse visual cortex as described previously (Ohki et al., 2005; Kerlin et al., 2010) by recording calcium responses to visual stimuli consisting of drifting gratings in each of 16 directions. We then acquired an *in vivo* fluorescent anatomical volume after injecting the tail vein with SR101 (100 mM) to label vasculature. The animal was perfused transcardially (2% paraformaldehyde/2.5% glutaraldehyde), and the brain was processed for serial-section TEM. Serial thin (<50 nm) sections were cut, picked up on Pioloform-coated slot grids, and then poststained with uranyl acetate and lead citrate. We imaged 1215 serial sections at 120 kV on a JEOL 1200 EX with a custom scintillator atop optical-quality leaded vacuum glass at the end of a custom-built vacuum chamber extension. Custom software controlled automated *x–y* stage motion and image acquisition with a 2 × 2 array of CCD cameras (Imperx IPX-11M5) (Imperx, Boca Raton, FL) and Zeiss lenses (Zeiss, Oberkochen, Germany). Images suitable for circuit reconstruction were acquired at a net rate of 5–8 megapixels per second. Camera images were aligned in two dimensions by registering adjacent camera images and dewarping, followed by histogram equalization and stitching. Then adjacent sections were registered and three-dimensional deformations were equalized in aligning the EM volume. Axonal and dendritic arbors of the functionally characterized neurons were manually reconstructed using TrakEM2, and objects were classified using classical criteria (Peters et al., 1991). Neurons or dendritic fragments receiving synapses from multiple functionally characterized cells were included in analysis of convergence. For each synapse participating in a convergence, a second individual (blind to the original reconstruction) traced the presynaptic and postsynaptic processes, starting from the synapse. Segmentation that diverged between the two tracers was excluded from further analysis. Cumulative synaptic proximity (CSP) of pairs of axons was calculated by centering a three-dimensional Gaussian density function at each synaptic bouton and taking the sum of their dot products over all pairs of synapses.

Acknowledgments

This paper was published in unabridged format in *Nature* (2011;471:177-182). Full methods and any associated references, as well as supplemental figures and movies, are available in the online version of the paper at www.nature.com/nature. We thank E. Raviola for discussions and technical advice on all aspects of EM; J. Stiles for support and advice concerning the alignment and stitching effort at the Pittsburgh Supercomputing Center; J. Lichtman for discussions and, along with K. Blum and J. Sanes, support from the Center for Brain Science; A. Cardona for help with TrakEM2, and many modifications of it; and H. Pfister and S. Warfield for discussions and help with computational issues. We also thank S. Butterfield for programming, and L. Benecchi and the Harvard Medical School EM Core Facility for technical support. For technical help with EM and its interpretation, we thank K. Harris, M. Bickford, M. Ellisman, K. Martin, and T. Reese. We thank J. Assad, R. Born, J. Maunsell, J. Stiles, E. Raviola, and members of the Reid laboratory for critical reading of the manuscript. This work was supported by the Center for Brain Science at Harvard University, Microsoft Research, and the National Institutes of Health through the National Eye Institute (NEI) to R.C.R. (EY10115 and EY18742), and through resources provided by the National Resource for Biomedical Supercomputing (P41 RR06009), which is part of the Pittsburgh Supercomputing Center, and by fellowships from Harvard Center for Neurodegeneration and Repair to D.D.B. and the NEI to W.-C.A.L. (EY18532).

NOTES

References

Ahmed B, Anderson JC, Martin KA, Nelson JC (1997) Map of the synapses onto layer 4 basket cells of the primary visual cortex of the cat. J Comp Neurol 380:230-242.

Alitto HJ, Dan Y (2010) Function of inhibition in visual cortical processing. Curr Opin Neurobiol 20:340-346.

Anderson JC, Douglas RJ, Martin KA, Nelson JC (1994) Map of the synapses formed with the dendrites of spiny stellate neurons of cat visual cortex. J Comp Neurol 341:25-38.

Anderson JR, Jones BW, Yang JH, Shaw MV, Watt CB, Koshevoy P, Spaltenstein J, Jurrus E, U V K, Whitaker RT, Mastronarde D, Tasdizen T, Marc RE (2009) A computational framework for ultrastructural mapping of neural circuitry. PLoS Biol 7:e1000074.

Binzegger T, Douglas RJ, Martin KA (2004) A quantitative map of the circuit of cat primary visual cortex. J Neurosci 24:8441-8453.

Braitenberg V, Schüz A (1998) Cortex: statistics and geometry of neuronal connectivity, 2nd ed. Berlin: Springer.

Dacheux RF, Raviola E (1986) The rod pathway in the rabbit retina: a depolarizing bipolar and amacrine cell. J Neurosci 6:331-345.

Denk W, Horstmann H (2004) Serial block-face scanning electron microscopy to reconstruct three-dimensional tissue nanostructure. PLoS Biol 2:e329.

Grewe BF, Helmchen F (2009) Optical probing of neuronal ensemble activity. Curr Opin Neurobiol 19:520-529.

Hamos JE, Van Horn SC, Raczkowski D, Sherman SM (1987) Synaptic circuits involving an individual retinogeniculate axon in the cat. J Comp Neurol 259:165-192.

Harris KM, Perry E, Bourne J, Feinberg M, Ostroff L, Hurlburt J (2006) Uniform serial sectioning for transmission electron microscopy. J Neurosci 26:12101-12103.

Hayworth K, Kasthuri N, Schalek R, Lichtman J (2006) Automating the collection of ultrathin serial sections for large volume TEM reconstructions. Microsc Microanal 12:86-87.

Helmstaedter M, Briggman KL, Denk W (2008) 3D structural imaging of the brain with photons and electrons. Curr Opin Neurobiol 18:633-641.

Heuser JE, Reese TS, Dennis MJ, Jan Y, Jan L, Evans L (1979) Synaptic vesicle exocytosis captured by quick freezing and correlated with quantal transmitter release. J Cell Biol 81:275-300.

Holmgren C, Harkany T, Svennenfors B, Zilberter Y (2003) Pyramidal cell communication within local networks in layer 2/3 of rat neocortex. J Physiol (Lond) 551:139-153.

Jia H, Rochefort NL, Chen X, Konnerth A (2010) Dendritic organization of sensory input to cortical neurons *in vivo*. Nature 464:1307-1312.

Kerlin AM, Andermann ML, Berezovskii VK, Reid RC (2010) Broadly tuned response properties of diverse inhibitory neuron subtypes in mouse visual cortex. Neuron 67:858-871.

Kisvárday ZF, Martin KA, Freund TF, Maglóczky Z, Whitteridge D, Somogyi P (1986) Synaptic targets of HRP-filled layer III pyramidal cells in the cat striate cortex. Exp Brain Res 64:541-552.

Liu BH et al. (2010) Intervening inhibition underlies simple-cell receptive field structure in visual cortex. Nature Neurosci 13:89-96.

Liu BH, Li P, Li YT, Sun YJ, Yanagawa Y, Obata K, Zhang LI, Tao HW (2009) Visual receptive field structure of cortical inhibitory neurons revealed by two-photon imaging guided recording. J Neurosci 29:10520-10532.

Ma WP, Liu BH, Li YT, Huang ZJ, Zhang LI, Tao HW (2010) Visual representations by cortical somatostatin inhibitory neurons—selective but with weak and delayed responses. J Neurosci 30:14371-14379.

Markram H, Lubke J, Frotscher M, Roth A, Sakmann B (1997) Physiology and anatomy of synaptic connections between thick tufted pyramidal neurones in the developing rat neocortex. J Physiol (Lond) 500:409-440.

Markram H, Toledo-Rodriguez M, Wang Y, Gupta A, Silberberg G, Wu C (2004) Interneurons of the neocortical inhibitory system. Nature Rev Neurosci 5:793-807.

Mason A, Nicoll A, Stratford K (1991) Synaptic transmission between individual pyramidal neurons of the rat visual cortex *in vitro*. J Neurosci 11:72-84.

McGuire BA, Gilbert CD, Rivlin PK, Wiesel TN (1991) Targets of horizontal connections in macaque primary visual cortex. J Comp Neurol 305:370-392.

Mishchenko Y, Hu T, Spacek J, Mendenhall J, Harris KM, Chklovskii DB (2010) Ultrastructural analysis of hippocampal neuropil from the connectomics perspective. Neuron 67:1009-1020.

NOTES

Niell CM, Stryker MP (2008) Highly selective receptive fields in mouse visual cortex. J Neurosci 28:7520-7536.

Ohki K, Reid RC (2007) Specificity and randomness in the visual cortex. Curr Opin Neurobiol 17:401-407.

Ohki K, Chung S, Ch'ng YH, Kara P, Reid RC (2005) Functional imaging with cellular resolution reveals precise micro-architecture in visual cortex. Nature 433:597-603.

Peters A, Kara DA (1985) The neuronal composition of area 17 of rat visual cortex. II. The nonpyramidal cells. J Comp Neurol 234:242-263.

Peters A, Palay SL, Webster HD (1991) The fine structure of the nervous system: neurons and their supporting cells, 3rd edition. New York: Oxford UP.

Ramón y Cajal S (1904) Textura del sistema nervioso del hombre y de los Vertebrados. Madrid: N. Moya.

Reynolds JH, Heeger DJ (2009) The normalization model of attention. Neuron 61:168-185.

Runyan CA, Schummers J, Van Wart A, Kuhlman SJ, Wilson NR, Huang ZJ, Sur M (2010) Response features of parvalbumin-expressing interneurons suggest precise roles for subtypes of inhibition in visual cortex. Neuron 67:847-857.

Shepherd GM, Harris KM (1998) Three-dimensional structure and composition of CA3RCA1 axons in rat hippocampal slices: implications for presynaptic connectivity and compartmentalization. J Neurosci 18:8300-8310.

Sohya K, Kameyama K, Yanagawa Y, Obata K, Tsumoto T (2007) GABAergic neurons are less selective to stimulus orientation than excitatory neurons in layer II/III of visual cortex, as revealed by *in vivo* functional Ca^{2+} imaging in transgenic mice. J Neurosci 27:2145-2149.

Song S, Sjøstrom PJ, Reigl M, Nelson S, Chklovskii DB (2005) Highly nonrandom features of synaptic connectivity in local cortical circuits. PLoS Biol 3:e68.

Sorra KE, Harris KM (1998) Stability in synapse number and size at 2 hr after long-term potentiation in hippocampal area CA1. J Neurosci 18:658-671.

Stepanyants A, Hirsch JA, Martinez LM, Kisvárday ZF, Ferecskó AS, Chklovskii DB (2008) Local potential connectivity in cat primary visual cortex. Cereb Cortex 18:13-28.

Sterling P (1983) Microcircuitry of the cat retina. Annu Rev Neurosci 6:149-185.

Stosiek C, Garaschuk O, Holthoff K, Konnerth A (2003) *In vivo* two-photon calcium imaging of neuronal networks. Proc Natl Acad Sci USA 100:7319-7324.

Tamas G, Somogyi P, Buhl EH (1998) Differentially interconnected networks of GABAergic interneurons in the visual cortex of the cat. J Neurosci 18:4255-4270.

Thomson AM, Bannister AP (2003) Interlaminar connections in the neocortex. Cereb Cortex 13:5-14.

Thomson AM, West DC, Wang Y, Bannister AP (2002) Synaptic connections and small circuits involving excitatory and inhibitory neurons in layers 2-5 of adult rat and cat neocortex: triple intracellular recordings and biocytin labelling *in vitro*. Cereb Cortex 12:936-953.

Tian L, Hires SA, Mao T, Huber D, Chiappe ME, Chalasani SH, Petreanu L, Akerboom J, McKinney SA, Schreiter ER, Bargmann CI, Jayaraman V, Svoboda K, Looger LL (2009) Imaging neural activity in worms, flies and mice with improved GCaMP calcium indicators. Nat Methods 6:875-881.

Turaga SC, Murray JF, Jain V, Roth F, Helmstaedter M, Briggman K, Denk W, Seung HS (2010) Convolutional networks can learn to generate affinity graphs for image segmentation. Neural Comput 22:511-538.

White EL, Keller A (1989) Cortical circuits: synaptic organization of the cerebral cortex — structure, function and theory. Boston: Birkhauser.

White JG, Southgate E, Thomson JN, Brenner S (1986) The structure of the nervous system of the nematode *Caenorhabditis elegans*. Phil Trans R Soc Lond B 314:1-340.

Yoshimura Y, Callaway EM (2005) Fine-scale specificity of cortical networks depends on inhibitory cell type and connectivity. Nature Neurosci 8:1552-1559.

Yoshimura Y, Dantzker JL, Callaway EM (2005) Excitatory cortical neurons form fine-scale functional networks. Nature 433:868-873.